Tuning of the Hydrophobic and Hydrophilic Interactions in 2D Chiral Domains

5 AUTHORS, INCLUDING:

Juan Giner-Casares

CIC biomaGUNE

46 PUBLICATIONS **283** CITATIONS

SEE PROFILE

Luis Camacho

University of Cordoba (Spain)

150 PUBLICATIONS **1,567** CITATIONS

SEE PROFILE

Tuning of the Hydrophobic and Hydrophilic Interactions in 2D Chiral Domains

Eugenio Jiménez-Millan,[†] Juan J. Giner-Casares,*[,†,‡] María T. Martín-Romero,[†] Gerald Brezesinski,[‡] and Luis Camacho*[,†]

[†]Department of Physical Chemistry, Campus de Rabanales, University of Córdoba, E-14014 Córdoba, Spain
[‡]Department of Interfaces, Max Planck Institute of Colloids and Interfaces, Science Park Golm, 14476 Potsdam, Germany

ABSTRACT: The molecular arrangement in the Langmuir monolayers is determined by the interplay of the hydrophilic and hydrophobic interactions between the components. Herein, the competition between the interactions of the components of the organic dye:phospholipid HSP:DMPA mixed monolayer has been studied. The HSP:DMPA monolayer gives rise to chiral domains at the air/solution interface. Brewster angle microscopy (BAM) has been used for the recording of the micrometric structure of the chiral domains. HSP absorb radiation at the wavelength of the laser used in BAM, providing information on the organization of the polar groups. The crystalline structure of the alkyl chains of the HSP:DMPA monolayer has been described by synchrotron-based grazing incidence X-ray diffraction. The interaction between alkyl chains dominates over the aggregation of the polar headgroup in the case of a pure water subphase. By simply adding ions in the subphase, this tendency is reversed, leading to a predominance of the aggregation of the polar headgroup, and a modification of the micrometric domains. This tuning of the interplay between the different molecular regions in a monolayer might be extended to different supramolecular systems, allowing the adjustment of the molecular arrangement.
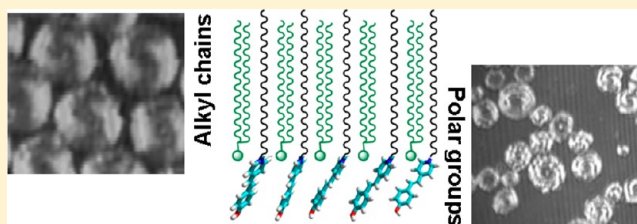
1. INTRODUCTION

The rationale design of supramolecular structures requires a delicate tuning of the intermolecular forces between the building blocks. The so-called interfacial supramolecular structures are assembled at an interface.[1] The interface provides a unique environment for the assembly process due to the imposed spatial constraints. The understanding of the assembly process at an interface is of maximum interest for the better understanding of the bulk self-assembly processes. Chiral interfaces are of high relevance, mainly in the following areas: heterogeneous catalysis using chiral recognition, and thin films devices for optical and electronic applications,[2] nanotechnology,[3] transfer of chirality from single molecules into supramolecular structures, and cooperatively driven chiral amplification phenomena.[4] Therefore, the engineering of the self-assembly process leading to supramolecular entities with chiral properties can greatly benefit from the use of an interface as the building environment. Indeed, the chirality in two dimensions (2D) has been the object of current intensive research.[5]

The detailed nature of the mechanisms of chirality transfer from the molecular to the supramolecular level is not completely understood. Moreover, the 2D supramolecular structures described so far are mostly only locally chiral, with both enantiomorphic domains statistically formed in equal amounts.[6] These supramolecular structures are therefore nonchiral, as they are composed of the same number of domains in both enantiomeric forms. The formation of supramolecular structures displaying exclusively one enatiomer

is of most relevance for the application of the supramolecular assemblies. A number of artificial receptor molecules, supramolecules, and π-conjugated macromolecules have been developed. Among them, achiral or dynamically racemic, but chromophoric supramolecular and macromolecular helical systems are particularly interesting. Upon noncovalent binding to a nonracemic guest, the chirality is transferred to the receptors, resulting in one of the enantiomeric or diastereomeric helical conformers, thus producing a characteristic induced circular dichroism (ICD) in the absorption region of the receptors.[7]

2D chiral films have been mainly studied at the air/solid interface. The air/solid interface is a rigid interface, providing a large degree of geometrical constraint. The rotational and translational motions of the molecules at the air/solid interface are restricted.[6] On the other hand, the air/liquid interface can be regarded as a soft surface. The molecules at the air/liquid interface have enhanced rotational and translational freedom when compared to the air/solid interface. Moreover, the air/liquid interface allows the displacement of the molecules in the z-axis, i.e., the perpendicular direction to the air/water interface plane, to a certain extent. The chirality in supramolecular assemblies at the air/water interface might be enhanced with respect to the air/solid interface. This enhancement is due to

Scheme 1. Left: Molecular Structures of 4-[4-Hydroxy)styryl]-1-docosylpyridinium Bromide (HSP) and Dimyristoylphosphatidic Acid (DMPA). Right: Scheme of the Mixed Langmuir Monolayer HSP:DMPA 1:1 at the Air/Liquid Interface
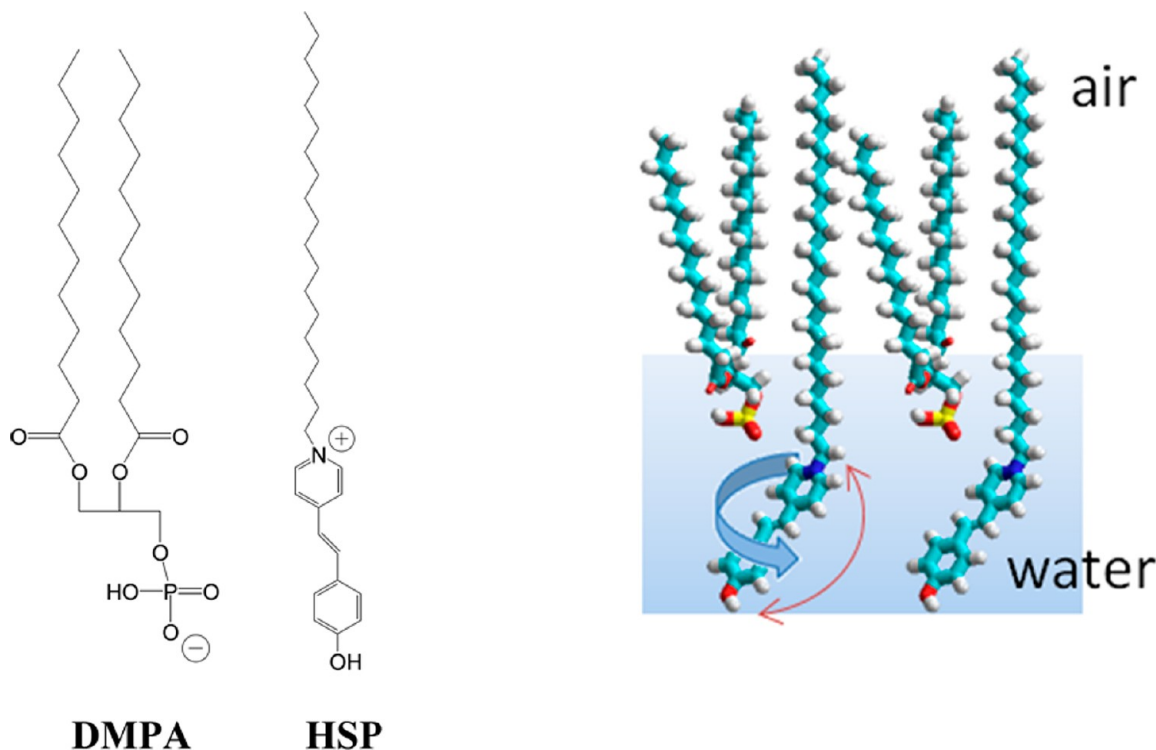
the long-range interactions, leading to the creation of domains in the micrometer scale. On the contrary, chiral supramolecular assemblies at the air/solid interface are restricted to a size of a few dozen nanometers.

A mixed Langmuir monolayer formed by two components has been studied herein. The two components are the anionic phospholipid DMPA and the cationic derivative of the hemicyanine dye HSP.[8] The molar ratio was 1:1. See Scheme 1 for the detailed molecular structures. The mixture is spread at the air/liquid interface to form a mixed Langmuir monolayer. The HSP:DMPA monolayer is stabilized at the air/liquid interface by the electrostatic interactions between the HSP and DMPA molecules. The available interfacial area for the dye moiety in the HSP molecule is ca. 0.6 nm^2 per HSP molecule. This value of area corresponds to three untilted alkyl chains: two alkyl chains per DMPA molecule plus one alkyl chain per HSP molecule. The surface area occupied by the alkyl chains is therefore larger than the surface area of the HSP headgroup. Given the shorter length of the alkyl chains of the HSP molecule than the DMPA molecule, the HSP headgroup has a large freedom to adopt different conformations, being able to display long-range aggregation.

Brewster angle microscopy (BAM) is the most useful tool to visualize and study the micrometric domains at the air/liquid interface. The BAM technique is based in the modification of the Brewster angle of the air/liquid interface upon covering of the interface with a Langmuir monolayer. This modification of the Brewster angle leads to the reflection of the incident laser light. The reflected light is captured by a camera, allowing the in situ visualization of the domains at the air/liquid interface. Herein, the use of BAM additionally comprises the enhanced reflection of incident radiation due to the absorption of the BAM laser (532 nm) by the headgroup of the HSP surfactant.[9]

2. EXPERIMENTAL SECTION

Materials. Hemicyanine dye, 4-[4-hydroxy)styryl]-1-docosylpyridinium bromide (HSP) and dimyristoylphosphatidic acid (DMPA) were purchased from Sigma-Aldrich and used as received. The molecular structures of DMPA and HSP are depicted in Scheme 1. Phosphate potassium and acetate sodium salts were purchased from Sigma-Aldrich. A mixture of chloroform:methanol, ratio 3:1 (v/v), was used as the spreading solvent for dissolving both HSP and DMPA. The pure solvents were obtained without purification from Aldrich. Ultrapure water, produced by a Millipore Milli-Q unit, pretreated by a Millipore reverse osmosis system (>18.2 MΩ/cm), was used as a subphase. For both buffer solutions, the concentration of salt in each case is 0.02 M. The pH was adjusted to pH = 6.6 by adding dropwise a solution of NaOH 1M. All experiments except GIXD were performed in a large class 100 clean room.

Methods. A Nima 601 Langmuir trough (Nima Technology, Coventry, England) provided with a Wilhelmy-type dynamometric system using a strip of filter paper has been used in this work. The NIMA 601 through is equipped with two symmetrical barriers. The monolayers were compressed at a speed of ca. 0.1 nm^2 min^{-1} molecule^{-1}. All the surface pressure—molecular area isotherms presented herein were performed at least three times, showing good reproducibility. No dependence of the number of molecules spread on the surface versus mean molecular area was observed for the different experiments. The temperature of the subphase was controlled by a recirculating water Lauda thermostat.

The monolayers were transferred onto quartz substrates, cleaned in successive steps with an alkaline detergent, isopropanol, and ethanol and then rinsed with ultrapure water. The monolayers were transferred at a constant surface

pressure by the Langmuir–Schaefer technique, i.e., by horizontal touching of the substrate at the interface covered with the mixed film. All transfers were performed at π = 30 mN/m. The ratio of the transfer process to the solid substrates was close to unity in all cases.

Images of the film morphology were obtained by Brewster angle microscopy (BAM) with a I-Elli2000 (Accurion GmbH), using a Nd:YAG diode laser with wavelength 532 nm and 50 mW, which can be recorded with a lateral resolution of 2 μm. The image processing procedure included a geometrical correction of the image, as well as a filtering operation to reduce interference fringes and noise. The microscope and the film balance were located on a table with vibration isolation (antivibration system MOD-2 S, Accurion GmbH).

The existence of chirality in the mixed monolayers is examined by CD spectroscopy of the transferred monolayers. A Jasco J-715 CD spectrophotometer has been used. All spectra were recorded at room temperature. The spectra were measured in the wavelength interval from 280 to 700 nm with a 0.2 nm step resolution and a 1 nm bandwidth. The scanning rate was 20 nm/min with 2 s response time. The signal-to-noise ratio was improved by accumulating 10 scans for each CD spectrum. Data processing was carried out using the J-700 software package. The blank spectrum of the bare quartz substrate was subtracted.

Grazing incidence X-ray diffraction measurements of the monolayer were performed at 21 °C at the BW1 beamline, HASYLAB, DESY (Hamburg, Germany). A Langmuir film balance equipped with a single movable barrier and a Wilhelmy plate for monitoring the lateral pressure was placed in a hermetically closed container filled with helium. At BW1, a monochromatic synchrotron X-ray beam (α = 1.304 Å) was adjusted to strike the helium/water interface at a grazing incidence angle α_i = 0.85α_c (α_c = 0.13°) and illuminated roughly 2 × 50 mm^2 of the surface. During the measurements, the trough was laterally moved to avoid any sample damage by the strong X-ray beam. A linear position-sensitive detector (PSD, MYTHEN, Switzerland) was rotated to scan the in-plane Q_{xy} component values of the scattering vector. The vertical channels of the PSD measured the out-of-plane Q_z component of the scattering vector between 0 and 0.8 Å^{-1}. The diffraction data consisted of Bragg peaks at diagnostic Q_{xy} values. The accumulated position-resolved counts were corrected for polarization, effective area, and Lorentz factor. Model peaks taken as Lorentzian in the in-plane direction and as Gaussian in the out-of-plane direction were least-squares fitted to the measured intensities. The diffracted intensity normal to the interface was integrated over the Q_{xy} window of the diffraction peak to calculate the corresponding Bragg rod. The thickness of the monolayer was estimated from the fwhm of the Bragg rod using ∼0.9(2π)/fwhm(Q_z). The cross-sectional area was calculated using homemade software taking into account the GIXD data.

3. RESULTS AND DISCUSSION

3.1. Surface Pressure–Area Isotherms and Brewster Angle Microscopy (BAM). In this work, we aim at the understanding of the intermolecular forces that lead to the formation of the chiral supramolecular domains and the further tuning of those interactions. The interplay of the lateral interactions between the alkyl chains and the lateral interactions between the polar groups is a topic of ongoing research with implications in the design of functional supramolecular

entities.[10] Herein, we aim at reaching the experimental conditions in which the morphology of the micrometric chiral domain can be tuned.

The HSP:DMPA monolayer has been formed at the air/liquid interface using ultrapure water at a temperature of 21 °C as the subphase. As previously described by Brewster angle microscopy, circular domains with inner chiral textures are observed.[8] Remarkably, the decrease of the temperature of the water subphase to 19 °C leads to no significant differences in the surface pressure–molecular area isotherms, whereas significant changes in the morphology of the domains are observed in this study, see Figure 1.
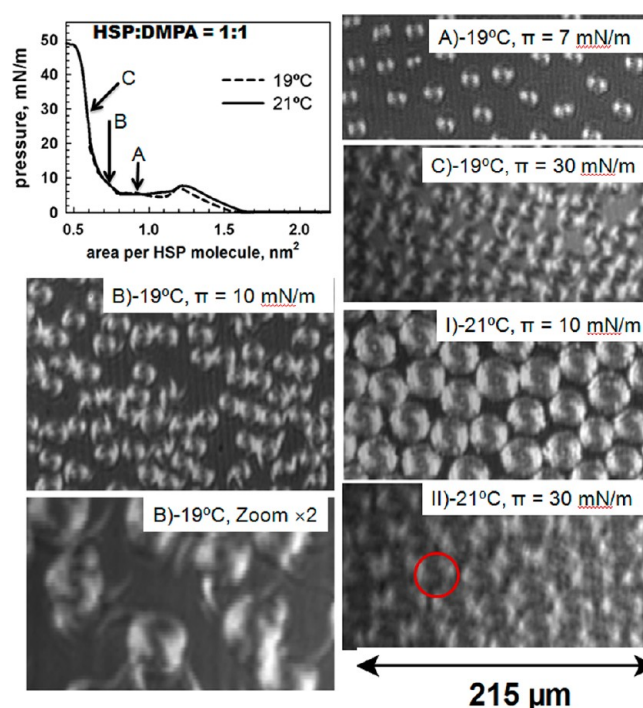

Figure 1. Top left: Surface pressure–molecular area isotherm of the mixed Langmuir monolayer HSP:DMPA at T = 19 °C and T = 21 °C, dotted line and solid line, respectively. (A, B, C) BAM pictures of the mixed Langmuir monolayer HSP:DMPA at T = 19 °C recorded at different values of surface pressure. Bottom right: BAM pictures of the mixed Langmuir monolayer HSP:DMPA at T = 21 °C recorded at a surface pressure of 10 mN/m (I) and 30 mN/m (II).

At 21 °C, the HSP:DMPA monolayer exhibits chiral domains with circular shape.[8] The diameter of the domains is ca. 20 μm, displaying internal structure; see Figure 1(I,II). This internal structure consists of a spiral dark region which resembles a helix, which crosses the domain vertically. The arms of the helix twist in the same direction for all domains, in a "S"-like fashion. Remarkably, this helical structure never rotates over 180° under the experimental conditions previously described.

Figure 1A−C shows the BAM images obtained for 19 °C. The size of the domains is reduced to approximately a half of the observed domains at 21 °C. The internal structure of the domains consists of a spiral dark region, similarly to the case at 21 °C. Branches grow from the circular domains at an area per HSP molecule of ca. 0.75 nm^2. See Figure 1B, down left BAM picture for a magnified view showing the branches. The brightness of the branches varies with the relative direction of their growth. The branches growing in the horizontal direction

are darker than the bright branches growing along the vertical direction. The director axis of the bright branches is coincident at the air/water interface plane with the polarization axis of the incident laser. The branches are bent as they grow from the circular structure. The curvature of the branches is in all the cases oriented anticlockwise. A deformation of the outer region of the circular domains with compression has been observed for the DMPA:HSP mixed monolayer at high surface pressures; see Figure 1(II). This deformation is likely provoked by the mechanical stress between the domains.

The addition of ions to the aqueous subphase leads to significant modification of the micrometric domains. The surface pressure−molecular area isotherm is similar for both subphases, with a modification of the overshoot toward a larger surface pressure for the phosphate subphase. Figure 2 shows
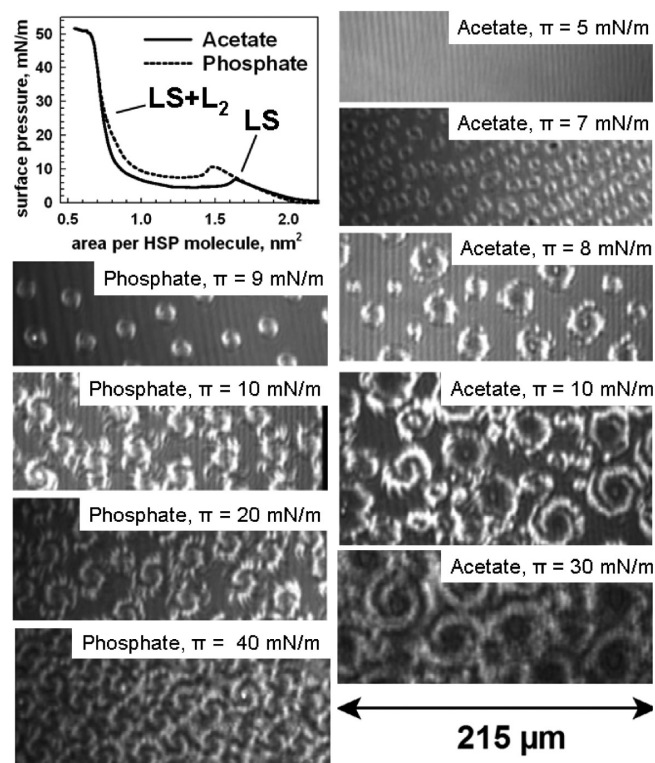

Figure 2. Top left: Surface pressure−molecular area isotherm of the mixed Langmuir monolayer HSP:DMPA in acetate and phosphate buffer solutions subphase, solid line and dotted line, respectively. The ionic concentration is 0.02 M, pH = 6.6. T = 21 °C. Left column: BAM pictures of the mixed Langmuir monolayer for phosphate buffer subphase at different values of surface pressure. Right column: BAM pictures of the mixed Langmuir monolayer for acetate buffer subphase at different values of surface pressure.

BAM pictures of the HSP:DMPA mixed Langmuir monolayer using either acetate or phosphate buffer solutions as a subphase. Acetate and phosphate buffers have been chosen for two main reasons. First, both buffers are widely available at a low cost, making the results presented in this study easy to be extrapolated to other systems by other researchers. Second, both the acetate and phosphate ions play a significant role in a large number of biophysical processes, therefore being of interest in the case of applying the described results herein to supramolecular systems with biophysical interest. For the expanded state of the monolayer, i.e., above the overshoot, the monolayer appears homogeneous. With the compression of the

monolayer, circular domains with internal anisotropy appear. The domains are similar to the domains previously described and shown in Figure 1 at low stages of compression. The domains grow spontaneously at constant surface pressure. Differently to the previous case, the circular domains are slightly deformed for values of surface area of ca. 1.0 nm^2 per HSP molecule. The deformation of the domains includes a certain loss of the circular shape and the appearance of branches from the outer edge of the domain. In spite of the deformation, the inner part of the domain keeps the inner structure with a spiral shape. This spiral shape resembles the shape of the branches observed for the HSP:DMPA monolayer on pure water subphase at low temperature. In both buffers, all the branches grow twisting toward the counterclockwise direction. For a surface pressure of ca. 10 mN/m, the circular shape of the domains is turned into spiral-like shapes. The shape of the domains is slightly modified form the circular shape to a spiral shape. This spiral shape is composed of two bright regions, which appears twisting around each other in the anticlockwise direction. Anticlockwise direction is assigned herein as the spiral is rotating to the left direction in all cases. The bright regions encircle a dark region, which occupies mainly the central region of the domains. This direction of growth is therefore opposite to that of the branches for the HSP:DMPA mixed monolayer on pure water subphase. With further compression of the monolayer, the distance within the domains decreases without coalescence. A similar behavior in these area regions has been observed in the presence of phosphate; see Figure 2. The size of the coils is slightly larger for the acetate than for the phosphate buffer. The domains on the phosphate buffer keep a limited size with compression of the monolayer smaller than in the case of the acetate buffer.

3.2. Circular Dichroism (CD) of LS Films. The domains resemble a chiral supramolecular structure. The HSP:DMPA mixed monolayer on both water and acetate subphase displays a circular dichroism signal after been transferred to a solid support; see Figure 3. The origin of the chirality in the domains
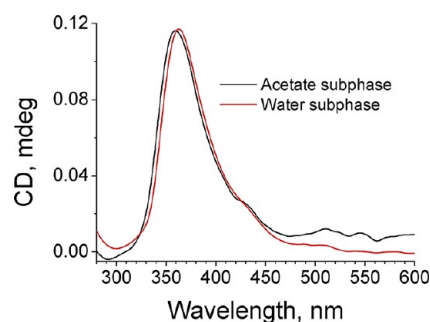

Figure 3. CD spectra of one HSP:DMPA mixed monolayer transferred to a quartz support by the Langmuir−Schaefer technique. Black line: HSP:DMPA mixed monolayer on 0.02 M acetate subphase. Red line: HSP:DMPA mixed monolayer on pure water subphase.

is related with the aggregation of the polar headgroups of the hemycianine. The hemicyanine groups might form chiral aggregates, as there is a certain degree of conformational freedom in the region below the alkyl chains. Hemicyanine is a prochiral group, therefore being able to form L- and R-chiral supramolecular structures.[11] The HSP:DMPA monolayer contains exclusively the L-isomer of DMPA, thus leading to exclusively one of the chiral isomers with the S-shape.[8] The origin of the CD signal is the aggregation of the HSP polar
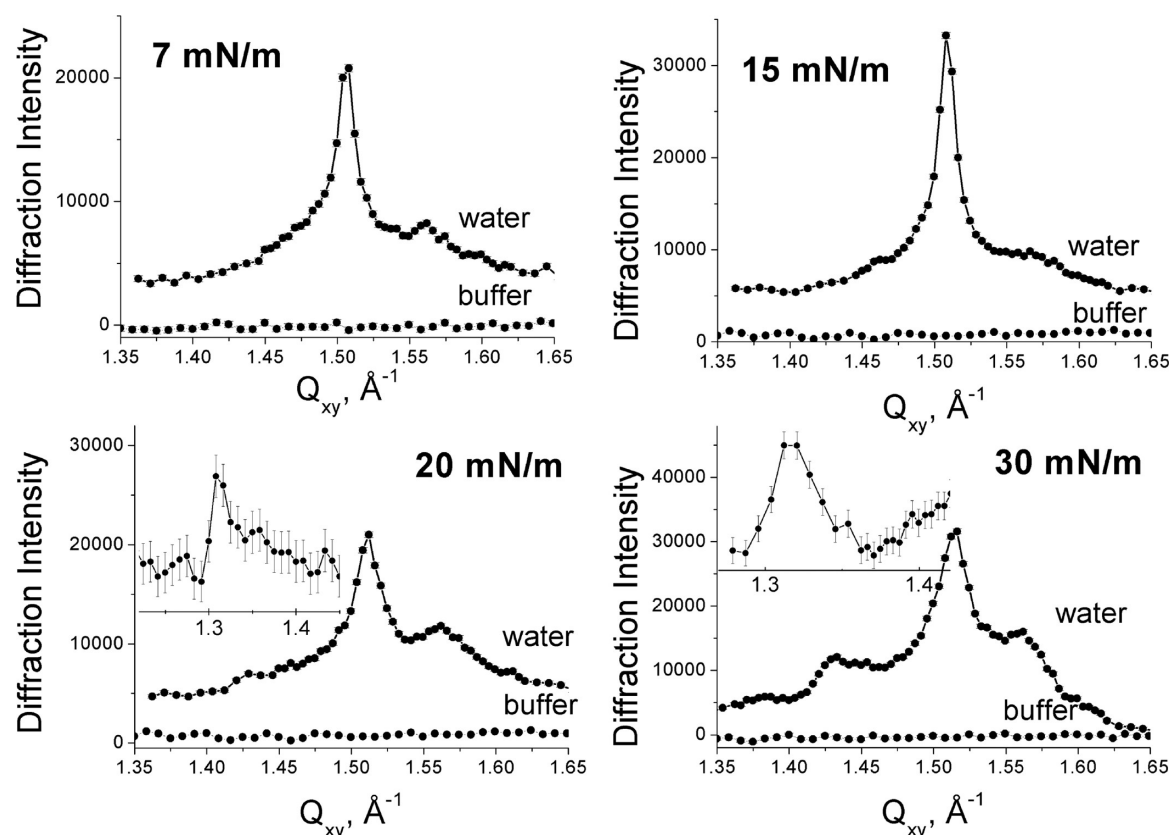
Figure 4. Bragg peaks for the mixed HSP:DMPA mixed monolayer in a molar ratio 1:1 at $T = 21$ °C. The GIXD signals obtained using pure water and acetate buffer are compared. Surface pressure values of 7, 15, 20, and 30 mN/m. Inset at 20 and 30 mN/m: magnification of the $Q_{xy} \sim 1.3$, related with the formation of H-bonds.
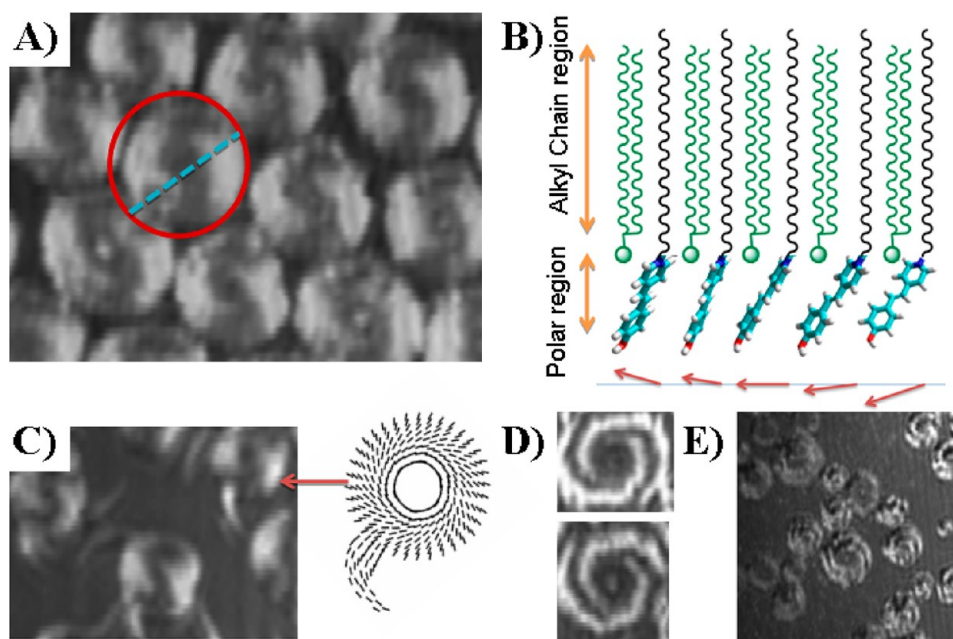

Figure 5. (A) Magnified BAM picture of the HSP:DMPA mixed monolayer on pure water subphase at $T = 21$ °C and 10 mN/m. The red circle marks the round shape of the domains. The dotted blue line indicates the diameter of the circle, ca. 20 μm. (B) Idealized scheme displaying the competing ordering of the alkyl chains and the aggregation of the hemycianine polar headgroup. (C) Magnified BAM picture of the HSP:DMPA mixed monolayer on pure water subphase at $T = 19$ °C and 10 mN/m. The adjacent drawing depicts the 2D network formed by the alkyl chains, this being a 2D network distorted within the branches. (D) Magnified BAM pictures of the HSP:DMPA mixed monolayer on acetate subphase at $T = 21$ °C and 10 mN/m. (E) BAM picture of the HSP:DMPA mixed monolayer on acetate subphase at $T = 21$ °C and 15 mN/m after six compression/decompression cycles.

Table 1. Primitive Unit Cell Parameters, Distortion Values, Tilt Angle, Projection of Hydrocarbon Chains in the *xy* Plane (A_{xy}) and Cross-Sectional Area of Hydrocarbon Chains (A_0) of the Mixed HSP:DMPA Monolayer in a Molar ratio 1:1 at T = 21 °C

			LS Phase		
π, mN m^{-1}	$a = b = c$, Å	$\alpha = \beta = \gamma$, deg	tilt angle, deg	$A_{xy} = A_0$, Å^2	L_{xy}, nm
7	4.817	120	0	20.1	33.2
15	4.811	120	0	20.0	31.4
20	4.798	120	0	19.9	20.2
30	4.792	120	0	19.8	20.2

				L_2' Phase				
π, mN m^{-1}	a, Å	$b = c$, Å	α, deg	$\beta = \gamma$, deg	distortion	tilt angle, deg	A_{xy}, Å^2	A_0, Å^2
30	5.228	4.808	114.1	122.9	0.1145	10.9	21.1	20.7

Table 2. In-Plane Q_{xy} and out-of-Plane Q_z Components of the Scattering Vector of the Mixed HSP:DMPA Monolayer in a Molar Ratio 1:1 at T = 21 °C[a]

	LS phase		L_2' phase			
π, mN m^{-1}	Q_{xy1}, Å^{-1}	Q_z, Å^{-1}	Q_{xy1}, Å^{-1}	Q_{z1}, Å^{-1}	Q_{xy2}, Å^{-1}	Q_{z2}, Å^{-1}
7	1.506 (0.017)	0 (0.313)	–			
15	1.508 (0.018)	0 (0.306)				
20	1.512 (0.028)	0	1.556 (0.053)	0.308 (0.260)	–	–
30	1.514 (0.028)	0	1.557 (0.052)	0.301 (0.323)	1.432 (0.033)	0 (0.385)

[a]The full width at half-maximum (fwhm) of the peaks is given in parentheses.

headgroups, as stated above. Indeed, the aggregation of the HSP polar headgroups is enhanced in the case of the HSP:DMPA mixed monolayer on a acetate buffer subphase. However, even for the case of a pure water subphase, the inner textures corresponding to the chiral supramolecular structures are present, as described herein. Therefore, the different degrees of the aggregation of the HSP polar headgroup lead to different morphologies of the domains, yet the supramolecular structure giving rise to chirality is essentially the same for all subphases..

3.3. Synchrotron Grazing Incidence X-ray Diffraction (GIXD). The understanding of the formation of chiral domains is aimed in terms of intermolecular aggregation. The internal structure of the circular domains shown by the HSP:DMPA mixed monolayer appears as a spiral dark region like a helix, which crosses the domain vertically. The arms of the helix twist in the same direction for all domains, in a "S"-like fashion. Surprisingly, on water subphase and for T = 21 °C, this helical structure never rotates over 180°; see Figure 5A. The achiral circular domain structure is maintained by lateral interactions between the alkyl chains, as shown herein by the GIXD data. The chirality in the internal structure of the domains is caused by the lateral aggregation of hemicyanine groups. This aggregation has been analyzed previously by simulations of the BAM images.[8] The interplay between the attractive interactions of the alkyl chains and the aggregation of the hemicyanine polar headgroup is discussed below.

The crystalline ordering of the hydrocarbon chains of the HSP and DMPA molecules can be analyzed by in situ grazing incidence X-ray diffraction (GIXD) using synchrotron-based radiation.[12] Note that the information at the nanometer scale provided by GIXD serves as complementary to the morphology of the domains described by BAM, which refers to the micrometric level. The information provided by BAM is herein related with the aggregated arrangement of the HSP polar headgroups, given the enhanced reflectivity of the HSP polar headgroups when compared to the alkyl chains.[9] On the other hand, the GIXD signal originates from the ordering of the alkyl

chains. The HSP polar headgroups display order for both subphases, with and without ions. Therefore, chiral supramolecular structures are observed by BAM. On the contrary, the ordering of the alkyl chains is only attained by using a pure water subphase, therefore the GIXD signal being exclusively present in the HSP:DMPA mixed monolayer on pure water subphase. The existence of ordered structures in the monolayer gives rise to Bragg peaks during the GIXD experiments. Remarkably, different diffraction patterns are observed during experiments of the HSP:DMPA on the pure water subphase; see Figure 4. On the contrary, in the presence of acetate buffer subphase, the mixed monolayer does not show scattering signal for any surface pressure analyzed. The information offered by GIXD cannot be used for deducing the morphology of the domains. The Bragg peaks for the HSP:DMPA mixed monolayer on water subphase indicates the existence of two crystalline phases: the LS and L_2' phases. The LS phase and L_2' have been related with the solid and liquid condensed phase of the Langmuir monolayers, respectively. The LS phase is present along the whole surface pressure−molecular area isotherm. The L_2' phase appears with the compression of the HSP:DMPA monolayer, and it is fully present for a surface pressure of 30 mN/m. The LS phase is characterized by a single Bragg peak at $Q_{xy} \sim 1.51$. Two Bragg peaks at $Q_{xy} \sim 1.56$ and $Q_{xy} \sim 1.43$ belong together to the L_2' phase. Although the Bragg peak at $Q_{xy} \sim 1.56$ can be observed at low values of surface pressure, the Bragg peak at $Q_{xy} \sim 1.43$ can be effectively characterized only at a large surface pressure of 30 mN/m. Therefore, a certain presence of the L_2' phase is assumed for the complete range of surface pressure, being relevant only at a high stage of compression. The positions of the Bragg peaks for both phases are shown in Table 2.

The well-defined micrometric circular domains observed by BAM for the HSP:DMPA mixed monolayer on water subphase appear at the surface pressure corresponding to the phase transition, ca. 7 mN/m. The alkyl chains show a highly organized crystal packing within the domains. The tight packing of the alkyl chains is characterized by the observed LS phase,

indicating a totally perpendicular orientation of the alkyl chains in the HSP:DMPA mixed monolayer. In other words, the alkyl chains are pointing completely upright from the plane of the air/water interface. A similar LS phase has been observed for the pure DMPA monolayer at high values of surface pressure.[13] The HSP:DMPA mixed monolayer is slightly distorted at high values of surface pressure. This distortion is observed as the contribution of a new crystalline L_2' phase to the GIXD signal, in which the alkyl chains are tilted with an angle of ca. 11°; see Table 1. On the other hand, the L_2' phase displays a tilting of the alkyl chains to the next-nearest neighbor (NNN), and distortion to the nearest neighbor (NN). The distortion is defined herein as the tilting of the azimuthal vector, perpendicular to the plane of the air/water interface. The quantitative parameters of the crystalline structures of the LS and L_2' phases are shown in Table 1. The untilted LS phase is present all along the isotherm of the HSP:DMPA mixed monolayer, regardless of the contribution of the L_2' phase.

The in-plane coherence length can be estimated from the full width at half-maximum (fwhm) of the Bragg peaks as approximately $L_{xy} \sim 0.9(2\pi)/\mathrm{fwhm}(Q_{xy})$. The fwhm of the Bragg peak belonging to the LS phase shows a brusque diminution from ca. 0.3 at 7 and 15 mN/m to ca. 0.2 at 20 and 30 mN/m. Despite the effective increase of packing of the alkyl chains with compression of the monolayer, leading to a reduction in the surface area (A_{xy}), the number of defects increases. Thus, according to the fwhm of the Bragg peak, ca. 60 alkyl chains can be found without defects at low values of surface pressure, while this value is reduced to ca. 40 alkyl chains without defects at high values of surface pressure. The introduction of defects might be related with the segregation of molecules from the LS phase to the L_2' phase, athough we cannot conclude this only from the GIXD data. The thickness of the monolayer (L_z) can be estimated from the full width at half-maximum (fwhm) of the Bragg rods by using the equation: $L_z \approx 0.9(2\pi)/\mathrm{fwhm}(Q_z)$. From the Bragg rods of the LS phase (Table 1), the thickness of the scattering centers, the alkyl chains, would be ca. 18 Å. Assuming an all-trans conformation for the hydrocarbon chains of the lipids, the length of a palmitoyl chain (C_{15}) from the DMPA lipid will be $L_{max} = (1.26 \times 14 + 1.5) = 19.1$ Å. Thus, a good agreement is obtained between the calculated thickness of the monolayer and the experimental value obtained by GIXD.

Remarkably, a small but significant Bragg peak at $Q_{xy} \sim 1.3$ is observed with a large density of molecules at the air/water interface, at a surface pressure higher than 15 mN/m. This Bragg peak has been related with the presence of H-bonds.[14] The GIXD peak corresponding to the H-bonds is observed in the HSP:DMPA mixed monolayer on water, but not on acetate buffer subphase. The H-bonds are exclusively observed for the HSP:DMPA mixed monolayer on a water subphase at high stages of compression of the monolayer. Therefore, the H-bonds might be related with the L_2' phase, given that both GIXD signals appear under the same conditions. In the case of the existence of H-bonds exclusively in the L_2' phase, the formation of intermolecular H-bonds through the OH groups of the hemicyanine dye could be favored by the deformation of the crystal lattice formed by the alkyl chains. In this scenario, the formation of such H-bonds would not be allowed in the LS phase, as this phase displays no deformation or tilting of the alkyl chain region. The molecular rotation within the crystalline structure of the alkyl chains might be hindered in the undistorted LS phase, therefore preventing the formation of a

2D row of H-bonds between the OH groups of the hemicyanine dye. On the other hand, given the weak GIXD signal produced by the H-bonds, there might be H-bonds already at low stages of compression, in the LS phase. In such a case, the low molecular density at the air/water interface would give a weak GIXD signal that might not be detected. With the present set of data, the formation of H-bonds cannot be unambiguously related with the appearance of the L_2' phase in the HSP:DMPA mixed monolayer. The appearance of intermolecular H-bonds is not relevant for the formation of the chiral supramolecular structures.

3.4. Polar versus Alkyl Chain Intermolecular Interaction. The formation of hydrogen bonds cannot be related to the growth of branches from the domains. For the case of the HSP:DMPA mixed monolayer on pure water subphase, the number of branched structures at 21 °C is quite small, while at 19 °C branched structures are formed mainly in the region corresponding to the phase transition, ca. 7 mN/m. The size and number of branches do not grow significantly when the surface pressure increase above 10 mN/m, while the hydrogen bonds are observed only when the surface pressure increases above 15 mN/m. For the case of the HSP:DMPA mixed monolayer on acetate buffer subphase, a large number of branches is observed, whereas no GIXD signal from H-bonds has been observed.

The different behavior of the HSP:DMPA mixed monolayer on either pure water or buffer subphase can be explained in terms of the competition between the intermolecular interactions as follows.

1. *HSP:DMPA Mixed Monolayer on Pure Water Subphase.* The lateral interactions between the alkyl chains are more relevant than the aggregation of the hemicyanine polar headgroups; see Figure 5A,B. The in-plane rotation of the HSP molecules is restricted by the tight arrangement of the alkyl chain in the HSP:DMPA mixed monolayer. This hindered rotation prevents the rotation of the helical structure formed by the hemicyanine polar headgroups to a larger value than 180°. For a diameter of the domain of 20 μm, and a separation between HSP molecules of 0.8 nm, ca. 25000 HSP molecules will exist along the diameter of the domain; see blue points line in Figure 5A. For a rotation angle of the inner texture within the domain of 180°, the average rotation per HSP molecule is 0.0072°. In the case of a temperature of 19 °C, branches start growing from the outer region of the circular domains. The branches are bent, with the curvature pointing to the same direction, anticlockwise. The aggregation of the hemicyanine polar groups induces the bending of the branches. The alkyl chains within the branches are assumed to rotate over 180°, therefore being segregated from the circular domains. The branches coming out from the circular domains are therefore originated from the dislocation of the 2D crystalline lattice formed by the alkyl chains, as schematically shown in Figure 5C.

2. *HSP:DMPA Mixed Monolayer on Acetate or Phosphate Subphase.* Circular domains with internal structure are formed similarly as in the previous case for larger areas than the overshoot in the surface pressure−molecular area isotherm; see Figure 2. The helicoidal internal structure of the domains is observed or a smaller size of the domain than using pure water as a subphase, indicating a greater angle of rotation per hemicyanine polar headgroup. A large number of branches along the outer edges of the circular domains are observed along the phase transition at a surface pressure of ca. 10 mN/m.
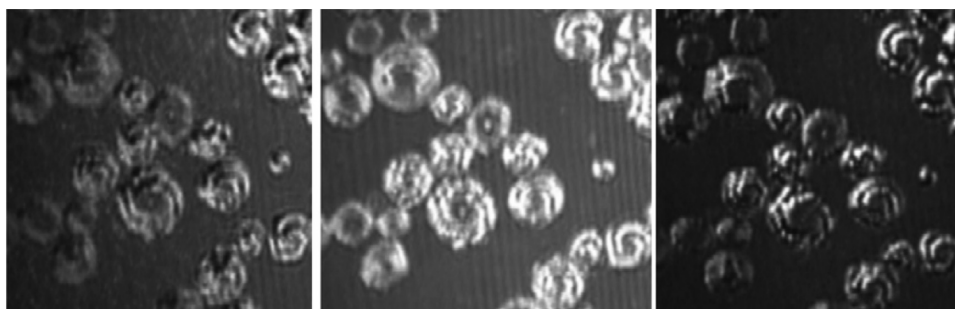
Figure 6. BAM pictures of the HSP:DMPA mixed monolayer on acetate subphase at $T = 21$ °C and 15 mN/m after six compression/decompression cycles. The angles of the polarizers of the BAM instruments were varied to improve the resolution in the texture of the domains. Left: polarizer = analyzer = 0°. Center: polarizer = −30°, analyzer = 0°. Right: polarizer = 30°, analyzer = 0°.

An apparent breaking of the circular structure of the domains is observed with compression of the monolayer, leading to spiral structures formed by two bright regions rotating around themselves. The spiral structures grow in the clockwise direction. There is no breaking of the circular structure of the domains, as proved by a detailed analysis of the BAM pictures. The HSP:DMPA mixed monolayer was subjected to six cycles of compression to 20 mN/m and decompression to 15 mN/m. The use of the successive compression/decompression cycles is aimed at the controlled growth of the domains, avoiding the growth and aggregation of the domains. Herein the preserved circular structure of the domains is seen, with the crisscrossed bright and the dark spirals. Additional BAM pictures are shown in Figure 6. Therefore, circular domains with chiral internal structure are formed, as in the previous case. However, the helical structure shows a rotation angle exceeding 180°; see Figures 5D,E, and 6. The rotation of the hemicyanine polar headgroup over 180° can occur exclusively in the case of free in-plane rotation of the alkyl chains of the HSP:DMPA mixed monolayer. Note that the interactions within the alkyl chains are still significant in maintaining the circular structure of the domains. On the other hand, the interactions between the hemicyanine polar headgroups are predominating. For the HSP:DMPA mixed monolayer on pure water subphase, the alkyl chains are arranged with a certain degree of rotation, as described for the rotator phase crystals. In this case, the rotation does not distort the crystalline structure of the alkyl chains. Therefore, the not distorted LS and the low distorted L_2' phases appear. On the contrary, for the HSP:DMPA mixed monolayer on acetate buffer subphase, the rotation of the alkyl chains is enhanced by the aggregation of the HSP polar headgroups, leading to a significant distortion of the crystalline lattice of the alkyl chains. This distortion occurs in a large extent, leading to the disruption of any crystallite of a size enough to give a GIXD signal. The freedom of the rotation of the alkyl chains involves the breaking of the crystalline lattice formed by the alkyl chains, which is indeed observed by GIXD, as described previously.

4. CONCLUSIONS

The aggregation of the hemicyanine polar headgroups is able to overcome the rotational constraints imposed by the lateral interactions between the alkyl chains. Therefore, the domains display spiral inner textures with rotation angles exceeding 180°. The increase of the interaction energy between hemicyanine polar headgroups is provoked by the ions present in the subphase. According to the results concerning acetate and phosphate ions, this phenomenon appears as a nonspecific ionic effect. Given that the aggregation of the hemicyanine dye is related with hydrophobic interactions, the use of salts in the subphase creates an ionic environment favoring aggregation of the dyes.

Chiral structures from the HSP:DMPA mixed monolayer have been formed at the air/solution interface. The molecular arrangement of the HSP and DMPA building blocks has been described by combining in situ microscopy and diffraction data. The interplay between the hydrophobic interactions of the alkyl chains and the aggregation of the hemicyanine polar head-groups leads to different mesoscopic arrangements. This interplay can be effectively tuned by simply adding ions in the aqueous subphase. Therefore, this method is proposed for the rationale modification of the molecular arrangement of a 2D monolayer via the adjustment of the intermolecular interactions.

■ AUTHOR INFORMATION

Corresponding Author

*E-mail: jjginer@uco.es (J.J.G.C.); lcamacho@uco.es (L.C.).

Notes

The authors declare no competing financial interest.

■ REFERENCES

(1) Vos, J. G.; Forster, R. J.; Keyes, T. E. *Interfacial Supramolecular Assemblies*; John Wiley & Sons: New York, 2003.

(2) Ernst, K.-H. Supramolecular Surface Chirality. *Top. Curr. Chem.* **2006**, *265*, 209−252.

(3) De Feyter, S.; De Schryver, F. C. *Chem. Soc. Rev.* **2003**, *32*, 139−150.

(4) Maeda, K.; Yashima, E. *Top. Curr. Chem.* **2006**, *265*, 47−88.

(5) Roth, C.; Parschau, M.; Ernst, K.-H. *ChemPhysChem* **2011**, *12*, 1572−1577.

(6) Fasel, R.; Parschau, M.; Ernst, K.-H.. *Nature* **2006**, *439*, 449−452.

(7) Ribó, J. M.; Crusats, J.; Sagués, F.; Claret, J.; Rubires, R. *Science* **2001**, *292*, 2063−2066.

(8) Jiménez-Millan, E.; Giner-Casares, J. J.; Martín-Romero, M. T.; Brezesinski, G.; Camacho, L. *J. Am. Chem. Soc.* **2012**, *133*, 19028−19031.

(9) Roldán-Carmona, C.; Giner-Casares, J. J.; Pérez-Morales, M.; Martín-Romero, M. T.; Camacho, L. *Adv. Colloid Interface Sci.* **2012**, *173*, 12−22.

(10) Giner-Casares, J. J.; Brezesinski, G.; Möhwald, H.; Landsmann, S.; Polarz, S. *J. Phys. Chem.Lett.* **2012**, *3*, 322−326.

(11) Vidal, F.; Delvigne, E.; Stepanow, S.; Lin, N.; Barth, J. V.; Kern, K. *J. Am. Chem. Soc.* **2005**, *127*, 10101−10106.

(12) Kjaer, K.; Als-Nielsen, J.; Helm, C. A.; Tippman-Krayer, P.; Möhwald, H. *J. Phys. Chem.* **1989**, *93*, 3200−3206.

(13) González-Delgado, A. M.; Rubia Payá, C.; Roldán-Carmona, C.; Giner-Casares, J. J.; Pérez-Morales, M.; Muñoz, E.; Martín-Romero, M. T.; Camacho, L.; Brezesinski, G. *J. Phys. Chem. C* **2010**, *114*, 16685−16695.

(14) Lepère, M.; Chevallard, C.; Brezesinski, G.; Goldmann, M.; Guenoun, P. *Angew. Chem., Int. Ed.* **2009**, *48*, 5005−5009.

19933

dx.doi.org/10.1021/jp307755a | *J. Phys. Chem. C* 2012, 116, 19925−19933